# Cross-Dataset Validation of a Sensor Agnostic Seismocardiography Peak Detection Method

Ismail Elnaggar†
Department of Computing
University of Turku
Turku, Finland
imelna@utu.fi

Sepehr Seifizarei
Department of Computing
University of Turku
Turku, Finland
seseif@utu.fi

Jonas Sandelin
Department of Computing
University of Turku
Turku, Finland
jojusan@utu.fi

Olli Lahdenoja
Department of Computing
University of Turku
Turku, Finland
olanla@utu.fi

Antti Airola
Department of Computing
University of Turku
Turku, Finland
ajairo@utu.fi

Matti Kaisti
Department of Computing
University of Turku
Turku, Finland
mkaist@utu.fi

Tero Koivisto
Department of Computing
University of Turku
Turku, Finland
tejuko@utu.fi

## ABSTRACT

Seismocardiography (SCG) is a non-invasive technique for capturing the mechanical vibrations of the heart, typically measured using inertial measurement units (IMUs) placed directly on the sternum, and offering insights into cardiac function beyond traditional electrocardiography. In this study, a novel SCG peak detection method is proposed that involves a multi-step rule-based algorithm. These detected peaks are then compared to the true R-peaks detected from time-synchronized ECG signals.

The method proposed in this study was evaluated using five publicly available datasets, N = 235 subjects. The heterogeneous nature of these datasets allowed for assessment of the proposed peak detection algorithm under varying signal quality conditions and clinical scenarios. Results indicate that the proposed method demonstrates high precision in peak detection across presumed healthy subject datasets with different sensor set ups and measurement protocols, with a mean sensitivity (TPR), precision (PPV), and interbeat interval root mean square error (RMSE) of 96.46%, 97.42%, and 40.64 ms for healthy subjects. Performance shows a notable decline in subjects with valvular heart disease: TPR, PPV, RMSE: 86.17%, 92.73%, and 121.7 ms and in subjects where measurements were taken during a right heart catheter procedure TPR, PPV, RMSE: 71.39%, 79.65%, and 183.1 ms.

This is the first such study using five open access SCG datasets together for validation of a SCG based peak detection method. All code and results have been open-sourced and are available on GitHub to foster reproducibility and further research in the community.

†Corresponding Author

CHASE '25, June 24–26, 2025, New York, NY, USA

ACM ISBN 979-8-4007-1539-6/2025/06.
https://doi.org/10.1145/3721201.3724416

## CCS CONCEPTS

• Applied computing → Life and medical sciences → Health informatics

## KEYWORDS

Seismocardiography, Peak Detection, Algorithm Design, Non-Invasive Cardiac Monitoring

**ACM Reference format:**

Ismail Elnaggar, Sepehr Seifizarei, Jonas Sandelin, Olli Lahdenoja, Antti Airola, Matti Kaisti, and Tero Koivisto. 2025. Cross-Dataset Validation of a Sensor Agnostic Seismocardiography Peak Detection Method. In *Proceedings of* 2025 IEEE/ACM Conference on Connected Health: Applications, Systems and Engineering Technologies *(CHASE'25). ACM, New York, NY, USA, 6 pages.* doi: 10.1145/3721201.3724416

## 1 Introduction

Seismocardiography (SCG) has in the last decade garnered increased attention as a non-invasive technique for monitoring cardiac mechanical activity by capturing chest wall vibrations produced by heartbeats. Unlike electrocardiography (ECG), which measures the electrical activity of the heart, SCG provides direct information about the mechanical events within the cardiac cycle, such as aortic valve opening (AO) and closure (AC) as well as other cardiac time intervals. Several studies have contributed methods for SCG based peak detection with the purpose of detecting aortic valve openings, calculate heart rate, heart rate variability, or other cardiac time intervals. Zheng et al. [1] proposed an approach that combines advanced filtering and successive variational mode decomposition (SVMD) to isolate AO peaks with high accuracy. Tadi et al. [2] introduced an adaptive heartbeat detection algorithm based on the S-transform, which leverages time–frequency analysis

to distinguish heartbeat events from background noise. Mora et al. [3] presented a comprehensive framework for the detection and analysis of heartbeats in SCG signals, detailing both the extraction and subsequent analysis of inter-beat intervals. Mann et al. as well as other researchers [4], [5], [6] have investigated methods to calculate different cardiac time intervals such as left ventricle ejection time (LVET), which has been shown to identify impaired cardiac function [7]. Kaisti et al. [8] and D'Mello et al. [9] addressed the challenges of standalone mechanocardiogram (MCG) heartbeat detection by utilizing multidimensional MCGs. Their studies explored the integration of multi-axis accelerometer data to improve the identification of cardiac events. Hurnanen et al. [10] investigated the use of dynamic balancing of multidimensional cardiac motion signals to enhance heartbeat detection accuracy. Choudhary et al. [11] demonstrated the application of variational mode decomposition for standalone heartbeat extraction, offering an approach that separates SCG signals into constituent modes to isolate heartbeats. Template matching techniques have shown promise in SCG beat detection applications as well. Centracchio et al. [12] introduced a template matching method for ECG-free heartbeat detection that employs normalized cross-correlation to identify heartbeats in SCG signals. Recent advances in deep learning have also been applied to SCG analysis. For example, Chen et al. [13] employed a bidirectional long short-term memory (BiLSTM) network for beat-to-beat heart rate detection, illustrating how neural networks can also capture the temporal dependencies present in SCG signals to recreate ECG signals.

Despite these contributions, most methods have been evaluated on a limited number of datasets, often from homogeneous subject populations. In this study, we propose a new method for SCG peak detection. To the best of our knowledge, this is the first time a SCG peak detection method has been validated across five open-access datasets together. The five datasets are: the Mechanocardiograms with ECG Reference dataset [14], the Combined measurement of ECG, Breathing and Seismocardiograms (CEBS) dataset [15], the Multichannel Seismocardiography dataset [16], the open-access VHD dataset [17], and the SCG-RHC Wearable dataset [18]. By testing our approach on these varied datasets, we aim to address limitations in past studies and investigate how well the proposed method generalizes across diverse recording conditions and subject demographics.

# 2 Materials

## 2.1 Open Access Datasets

To properly validate the performance of the proposed peak detection algorithm requires thorough validation across diverse sensor configurations and patient populations. To address this objective, five open access datasets have been assembled for evaluating the method proposed in this study. These datasets have been summarized in Table 1 below. Each dataset was recorded using a unique sensor setup and protocol. For this analysis, all datasets were resampled to 200 Hz for consistent processing. Three of the datasets involve presumed healthy participants, while the remaining two include individuals with a history of cardiovascular disease. Each dataset used a different sensor setup and measurement protocol allowing these five datasets to provide a comprehensive basis for assessing the proposed methods performance under varying physiological and technological conditions. In order to include as much data as possible in this study, the Z-axis SCG signal was the only axis considered. This was because it was the only axis of measurement all five datasets shared in common. Some datasets contained more than one ECG lead. In that case, the lead that produced the best signal based on visual inspection was chosen for each dataset to be used as the ground true R-peak source. The Multichannel SCG dataset [16] contained data from 16 tri-axis accelerometers. The Z-axis signal with the coordinates (2, 3) was used in this study. For more information on the datasets used in this study please refer to the relevant dataset citations.

**Table 1: Dataset Summary**

| Dataset | N | Age | Males | Height | Weight |
|---|---|---|---|---|---|
| [14] | 29 | 29 ± 5 | 29 | 179 ± 5 | 76 ± 11 |
| [15] | 20 | 24.7 ± 3.9 | 11 | NA | NA |
| [16] | 13 | 27 ± 4 | 13 | NA | NA |
| [17] | 100 | 68 ± 14 | 59 | 165 ± 9 | 69 ± 13 |
| [18] | 73 | 55.53 ± NA | 49 | 172.35 ± NA | 87.83 ± NA |

## 2.2 Signal Processing Pipeline

The algorithm begins by preprocessing the SCG Z-axis signal through subtracting the mean from the signal and band-pass filtering from 10 to 30 Hz to remove baseline wander and high-frequency noise. The filtered signal is then raised to the fourth power, in order to accentuate the aortic opening complexes, making them more prominent. The signal then is segmented into 10-second windows with overlapping extensions to mitigate edge effects during subsequent analysis. Each window is then decomposed using a variant of SVMD [1], [19], which separates the signal into intrinsic modes representing underlying physiological processes and noise.

Following the decomposition, a subset of the modes are recombined to reconstruct a signal that predominantly reflects aortic opening events. This reconstructed signal is further normalized and filtered with a secondary band-pass filter (5-35 Hz) to eliminate any remaining baseline wandering produced by the SVMD process. Next, the algorithm applies an improved version of a continuous wavelet transform (CWT) based envelope creation method developed in an earlier work from [20]. The transform is applied to the reconstructed signal by computing the CWT using the Morlet wavelet across a predefined set of scales, which creates a time-scale representation of the signal. This representation is then smoothed by applying a symmetric two-dimensional convolution with triangular windows, effectively reducing noise while preserving the signal information related to cardiomechanical activity. The smoothed CWT is further refined through a stepped thresholding procedure, wherein sliding windows (approximately 500 ms and 350 ms in duration with specific overlaps) are used to

compute dynamic thresholds based on the interquartile range and maximum value of the CWT coefficient values.

Subsequently, a one-dimensional envelope is generated by extracting the maximum value across scales at each time point, followed by additional smoothing via convolution with triangular windows approximating 300 ms and 100 ms durations. The envelope is then normalized, and a peak detection algorithm based on the Automatic Multiscale-based Peak Detection (AMPD) [21] method is applied to accurately identify the temporal locations of the aortic opening peaks. This multi-stage CWT-based approach, combining smoothing and adaptive thresholding techniques, attempts to isolate the cardio-mechanical events in the SCG signal associated with AO events. These detected peaks were then compared with the corresponding ECG R-peaks. ECG R-peaks were detected using the default peak detection algorithm present in the neurokit2 python package [22].

*2.2.1 Successive Variational Mode Decomposition*

The SVMD-based method implemented in this study iteratively decomposes a univariate signal $x(t)$ with $(t = 1, \dots, N)$ into a set of intrinsic mode functions (IMFs) by successively extracting modes that capture dominant oscillatory components. Initially, the residual $r(t)$ is set equal to the input signal. For each mode $m_k(t)$, an iterative procedure is employed that updates the mode estimate in the frequency domain using a approximated Wiener filtering approach. At each iteration, $j$, the mode is updated as follows:

$$m_k^{(j+1)}(t) = \mathcal{F}^{-1}\left\{\frac{\mathcal{F}\left\{r(t) - m_k^{(j)}(t) + \frac{1}{2}\lambda_k^{(j)}(t)\right\}}{1+\alpha(2\pi f)^2}\right\} \qquad (2.1)$$

where $\mathcal{F}$ and $\mathcal{F}^{-1}$denote the Fourier and inverse Fourier transforms, $f$ represents the frequency, and α is a predefined regularization parameter that controls the smoothness of the extracted mode. Simultaneously, a Lagrange multiplier $\lambda_k(t)$ is updated using:

$$\lambda_k^{(j+1)}(t) = \lambda_k^{(j)}(t) + [r(t) - m_k^{(j+1)}(t)] \qquad (2.2)$$

which reinforces the constraint that the mode should capture a portion of the residual energy. This iterative update continues until the relative change in the mode, as measured by:

$$\frac{\|m_k^{(j+1)} - m_k^{(j)}\|}{\|m_k^{(j)}\|} < \epsilon \qquad (2.3)$$

Where $\|\cdot\|$ representing the Frobenius norm [23] drops below $\epsilon$ representing a predefined tolerance value. Once convergence is achieved for a mode, it is subtracted from the residual and stored. The algorithm then proceeds to extract the next mode until a maximum number of modes is reached or the residual energy becomes negligible.

For the reconstruction of the AO signal, each extracted mode is evaluated using a waveform factor, *wf,* defined as:

$$\mathrm{wf}(m_k) = \frac{\sqrt{\langle m_k(t)^2 \rangle}}{\langle |m_k(t)| \rangle} \qquad (2.4)$$

where $\langle \cdot \rangle$ denotes the temporal average. Modes with a waveform factor exceeding the average waveform factor across all modes are selected and summed to form the final reconstructed signal [1]. This selective reconstruction procedure attempts to select the modes that are most representative of the AO events, refining the signal for subsequent processing.

*2.2.2 Peak Detection Envelope Creation*

Once the reconstructed signal is produced a CWT is applied to the signal. The CWT–based approach begins by transforming the preprocessed, reconstructed SCG Z-axis signal, $x(t)$, into a time-scale representation using the Morlet wavelet. The CWT is given by:

$$W(a,b) = \frac{1}{\sqrt{a}}\int_{-\infty}^{\infty} x(t)\psi^*\left(\frac{t-b}{a}\right)dt \qquad (2.5)$$

where $a$ is the scale, $b$ is the time translation, and ψ is the Morlet wavelet. In this implementation, the CWT is computed for a set of discrete scales corresponding to the frequency band of 10 to 30 Hz with a 0.1 Hz spacing, and the absolute values of the coefficients are taken to emphasize the energy content at each time-scale pair. The 2D CWT coefficient matrix $W(a,b)$ is then smoothed using symmetric convolution. This smoothing is performed by convolving along both the scale and time axes with triangular windows, which can be described by:

$$\tilde{W}(a,b) = \sum_{a'} \sum_{b'} W(a',b')K_a(a-a')K_b(b-b') \qquad (2.6)$$

where $K_a$ and $K_b$ are triangular window functions defined over the scale and time dimensions, respectively. This two-dimensional smoothing attempts to reduce high-frequency artifacts. Following the symmetric smoothing, an adaptive, stepped thresholding strategy is applied to further refine the smoothed CWT coefficients. The time-scale matrix is partitioned into overlapping time windows with durations set to 500 ms and 350 ms, and within each window, two thresholds are computed. For the high-frequency coefficients, the threshold is based on the interquartile range (IQR):

$$T_{\mathrm{hf}} = \mathrm{IQR}\left(\tilde{W}_{\mathrm{hf}}\right) \times \mathrm{hf} \qquad (2.7)$$

and for the low-frequency (higher scale) coefficients, it is based on the maximum absolute value:

$$T_{\mathrm{lf}} = \mathrm{Max}\left(\tilde{W}_{\mathrm{lf}}\right) \times \mathrm{lf} \qquad (2.8)$$

with *hf* and *lf* being scaling factors. Coefficients that do not exceed these thresholds are set to zero, ensuring that only significant coefficients corresponding AO events are retained.

After thresholding, an envelope $e(b)$ is extracted by taking the maximum value across all scales at each time point:

$$e(b) = \max_a |\tilde{W}(a,b)| \qquad (2.9)$$

This envelope is then normalized and further smoothed through two successive convolutions with triangular windows, first with a window approximating 300 ms and then with another approximating 100 ms. Finally, the function employs an adaptive method based on the AMPD algorithm. This method identifies local maxima in the envelope $e(b)$ within a specified scale window, representing the temporal locations of AO events.

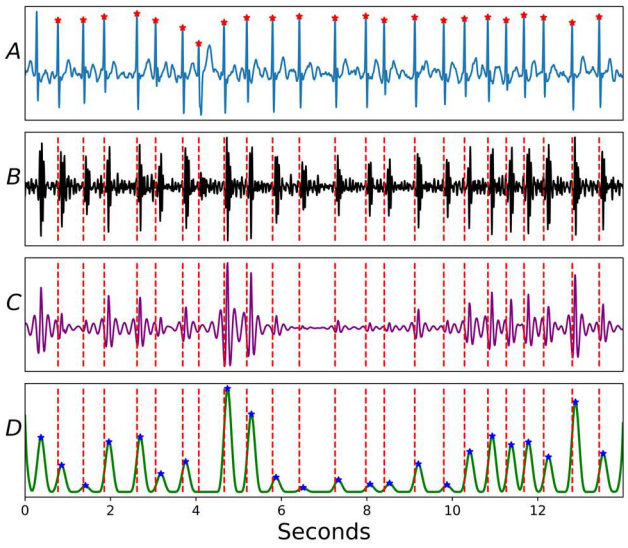


**Figure 1: Segment from the valvular heart disease dataset [17]. Plot A: 1-lead ECG, Plot B: Bandpass filtered z-axis SCG signal, Plot C: Output of the SVMD function, Plot D: Envelope signal used for peak detection. R-peaks are denoted by red *'s in plot A and with red vertical dashed lines in plots B, C, and D. Detected SCG peaks are denoted by blue *'s in plot D.**

## 3 Results

The performance of the presented algorithm were evaluated using synchronized reference ECG R-peaks with respect to the detected peaks and inter-beat intervals detected from the Z-axis SCG signal. The results for the SCG peak detection algorithm were calculated using a tolerance window of 250 ms. The tolerance window value of 250 ms was selected to account for the time synchronization differences between the SCG and ECG signals across the five datasets. For each detected peak position, $P_i$ with $(i = 1, \dots, M)$ , the following criteria are applied:

$$\text{True positive (TP): } \exists j: \left|\mathrm{P}_i - \mathrm{R}_j\right| \leq 250 \text{ ms}$$
$$\text{False positive (FP): } \nexists j: \left|\mathrm{P}_i - \mathrm{R}_j\right| \leq 250 \text{ ms}$$
$$\text{False negative (FN): } \nexists i: \left|\mathrm{P}_i - \mathrm{R}_j\right| \leq 250 \text{ ms}$$

where $\mathrm{R}_j$ is the reference R-peak. Based on these definitions, the sensitivity (true positive rate, TPR) and precision (positive predictive value, PPV) are calculated as follows:

$$\text{TPR (\%)} = \frac{\text{TP}}{\text{TP+FN}} \times 100 \qquad (3.1)$$

$$\text{PPV (\%)} = \frac{\text{TP}}{\text{TP+FP}} \times 100 \qquad (3.2)$$

The RMSE is computed as a measure of the temporal accuracy of the beat-to-beat intervals derived from the detected peaks relative to the reference intervals. For each reference beat $r_i$ , a corresponding candidate detected peak is first identified. If a true positive is available, that value is used. In the absence of a true positive, the algorithm searches within an extended window $[r_i - 250ms, r_{i+1}]$ and selects the peak nearest to $r_i$. For the last reference beat, if no true positive is found, a similar search is conducted within its true positive window. If no alternative beat is found within the extended window, that beat-to-beat interval is excluded from the RMSE calculation. Once a candidate $p_{\text{candidate}}[i]$ is determined for each reference beat $r_i$, the error for each adjacent pair of beats (where candidates for both beats are available) is calculated:

$$\text{RMSE} = \sqrt{\frac{1}{M}\sum_{i=0}^{M-1} (\text{error}_i)^2} \qquad (3.3)$$

In addition to the above metrics, heart rate was calculated using a two-second windowing. This heart rate calculation considered all peaks in both the ECG signal as well as the SCG signal and calculated an average heart rate value based on the peaks present in each two-second window. If no peaks were present for a given window in either the ECG or SCG signal, that heart rate window was interpolated using a linear interpolation. The ECG and SCG heart rates were then compared to produce a heart rate mean absolute error (HRMAE) metric.

**Table 2: Cross-Dataset Test Results**

| Data | TPR (%) | PPV (%) | TP | FP | FN | RMSE (ms) | HRMAE (BPM) |
|---|---|---|---|---|---|---|---|
| [14] | 94.01 | 95.29 | 545 | 20 | 24 | 57.3 | 2.05 |
| [15]B | 97.47 | 98.26 | 336 | 6 | 9 | 33.9 | 1.48 |
| [15]P | 97.49 | 98.30 | 337 | 5 | 8 | 33.1 | 1.41 |
| [15]M | 96.21 | 97.37 | 3361 | 83 | 126 | 41.7 | 1.74 |
| [16] | 97.15 | 97.99 | 299 | 5 | 7 | 37.2 | 1.43 |
| [17] | 86.17 | 92.73 | 476 | 33 | 83 | 121.7 | 8.78 |
| [18] | 71.39 | 79.65 | 1541 | 348 | 592 | 183.1 | 11.06 |

Table 2 presents a summary of the averaged results across all five datasets. For dataset [16], four subjects had to be excluded because of issues in their ECG recordings. One recording also had to be excluded from both dataset [17] and [18] because of similar issues. Dataset [15] results are presented with the letters, B, M, and P because each subject had three separate recordings taken. One before listening to music, one during listening to music, and one post listening to music. The aggregated mean TPR, PPV, RMSE, and HRMAE for the presumed healthy datasets [14], [15], [16] was 96.46%, 97.42%, 40.64 ms, and 1.62 bpm.

**Table 3: ECG Summary Statistics**

| Data | Mean ECG HR | Min ECG HR | Max ECG HR | STD ECG HR |
|---|---|---|---|---|
| [14] | 66.53 | 52.09 | 82.10 | 6.53 |
| [15]B | 69.26 | 55.15 | 96.13 | 8.86 |
| [15]P | 69.21 | 55.15 | 96.11 | 8.88 |
| [15]M | 70.21 | 55.53 | 100.40 | 9.74 |
| [16] | 70.31 | 46.73 | 82.90 | 11.34 |
| [17] | 77.02 | 46.91 | 155.80 | 16.34 |
| [18] | 79.52 | 54.61 | 111.60 | 12.59 |

**Table 4: Previous Works Comparison**

| Reference | Dataset | N | TPR (%) | PPV (%) |
|---|---|---|---|---|
| [12] | [17] | 77 | 96 | 97 |
| [24] | [17] | 76 | 90 | 91.5 |
| [25] | [15]B | 20 | 94 | 90 |
| [1] | [15]B | 20 | 99 | 99 |
| [1] | [15]M | 20 | 99.6 | 98.9 |
| [1] | [15]P | 20 | 99.4 | 99.4 |
| [26] | [15]B | 20 | 97.3 | 97.4 |
| *Proposed* | *[17]* | *99* | *86.2* | *92.7* |
| *Proposed* | *[15]B* | *20* | *97.5* | *98.3* |
| *Proposed* | *[15]P* | *20* | *97.5* | *98.3* |
| *Proposed* | *[15]M* | *20* | *96.2* | *97.4* |

## 4 Discussion

The detection algorithm was evaluated on seven recording sessions across five datasets. Datasets [14], [15], and [16] represent recordings from healthy subjects, while datasets [17] and [18] correspond to subjects with clinical conditions. Heart rate was computed using two-second windows based on peaks identified in both ECG and SCG signals while missing windows were linearly interpolated. The HRMAE was then determined by comparing the ECG and SCG heart rates.

For the healthy subject datasets, the aggregated results show a true positive rate (TPR) of 96.46% and a positive predictive value (PPV) of 97.42%, with an RMSE of 40.64 ms. These metrics indicate that the algorithm reliably identifies aortic opening peaks with low temporal error in healthy recordings. In contrast, the non-healthy datasets exhibit reduced performance. Dataset [17] shows a TPR of 86.17%, a PPV of 92.73%, an RMSE of 121.7 ms, and an HRMAE of 8.78 bpm. Dataset [18] further deteriorates with a TPR of 71.39%, a PPV of 79.65%, an RMSE of 183.1 ms, and an HRMAE of 11.06 bpm. The results demonstrate a clear difference in detection accuracy and temporal precision between healthy and non-healthy subject recordings. It is unclear how much the degraded performance of the algorithm on the RHC dataset [18] was due to the disease status of the subject or because of the active invasive right heart catheter procedure that was being conducted on the subjects at the time of measurement recording. As seen by Table 3, the average heart rate varied between datasets demonstrating that the proposed method in this study was evaluated over a large range of heart rates.

Table 4 summarized related works tested using either the CEBSDB [15] or the VHD dataset [17] against the method proposed in this study. Centracchio et al. and Parlato et al. [12], [24] both tested their methods using the VHD dataset and reported promising results. In both studies around 25% of the available subjects in the VHD were not considered. This could be one explanation in the difference in performance between the proposed method in this study and these related works. Zheng et al. and Choudhary et al. [1], [25], [26] proposed promising results in their studies that are in line with the method proposed in this study or preform slightly better but only validated their methods using one dataset, the CEBSDB [15]. To the best of our knowledge this is the first study that has used datasets [16], [18] for validation of a peak detection method.

In Figure 1, the proposed detection method was visualized using an example segment from a subject from the valvular heart disease dataset [17]. In plot D, the envelope plot, at the 4 second mark we can see that a false negative occurs because no peak was detected for that r-peak. Interestingly enough that peak was produced by an ectopic beat. It is very possible that because datasets [17], [18] contain older subjects who have a history of cardiac disease, that their signals contained more ectopic beats that could have caused a reduction in the performance of this algorithm. Many of these subjects also exhibited different arrhythmias during visual inspection of their ECG signals. These arrhythmias may make peak detection challenging because the AMPD algorithm expects to receive a quasi-periodic signal as the input. If many ectopic beats occur throughout the signal at random, they could be missed by the AMPD peak detection function.

The following limitations are present in this study. Only the Z-axis SCG signal was considered. This was done so because it was the only common access available across all datasets. Future work could possibly analyze each available SCG measurement axis's performance independently or the combined performance similarly to [8]. This dataset considered both subjects with and without a history of heart disease and showed differing performance between the two groups. It is still inconclusive if this difference in performance was due to the different disease status of the cohorts or because of the sensor set up and measurement protocol used in each study. In order to address this issue future work could attempt to collect a large dataset with a single type of sensor across different disease populations in order to quantify the impact of disease status on the accuracy of a given peak detection method. This would allow for a more robust analysis of a given method.

## 5 Conclusion

In summary, the results indicate that the proposed method demonstrates high precision in peak detection across presumed healthy subject datasets with different sensor set-ups and measurement protocols. Performance shows a notable decline in subjects with valvular heart disease and in subjects who had their measurements taken during a RHC procedure. These findings highlight the need for further investigation to refine the proposed approach, particularly to enhance its accuracy among older individuals and in individuals with a history of cardiovascular disease.

## Acknowledgements

This study was supported by the Chips Joint Undertaking (Grant Agreement No. 101095792) and its members Finland, Germany,

Ireland, the Netherlands, Sweden, Switzerland. This work includes top-up funding from the Swiss State Secretariat for Education, Research and Innovation (SERI).

## Appendix

The code for the method presented in this study can be found on github: https://github.com/IsmailElnaggar/CHASE2025_Cross_Dataset_SCG_Benchmark

## REFERENCES


[1] C. Zheng, W. Peng, T. Huang, Y. C. Eldar, and M. Yu, "High accurate detection method for aortic valve opening of seismocardiography signals," *Biomedical Signal Processing and Control*, vol. 87, p. 105484, Jan. 2024, doi: 10.1016/j.bspc.2023.105484.

[2] M. J. Tadi, E. Lehtonen, O. Lahdenoja, M. Pankaala, and T. Koivisto, "An adaptive approach for heartbeat detection based on S-transform in seismocardiograms," in *2016 38th Annual International Conference of the IEEE Engineering in Medicine and Biology Society (EMBC)*, Orlando, FL, USA: IEEE, Aug. 2016, pp. 2370–2373. doi: 10.1109/EMBC.2016.7591206.

[3] N. Mora, F. Cocconcelli, G. Matrella, and P. Ciampolini, "Fully Automated Annotation of Seismocardiogram for Noninvasive Vital Sign Measurements," *IEEE Trans. Instrum. Meas.*, vol. 69, no. 4, pp. 1241–1250, Apr. 2020, doi: 10.1109/TIM.2019.2908511.

[4] A. Mann, M. M. Rahman, V. Vanga, P. T. Gamage, and A. Taebi, "Variation of Seismocardiogram-Derived Cardiac Time Intervals and Heart Rate Variability Metrics Across the Sternum," *Journal of Medical Devices*, vol. 18, no. 4, p. 044502, Dec. 2024, doi: 10.1115/1.4066368.

[5] I. Elnaggar *et al.*, "Cardiac Time Intervals Derived from Electrocardiography and Seismocardiography in Different Patient Groups," in *2022 Computing in Cardiology (CinC)*, 2022, pp. 1–4. doi: 10.22489/CinC.2022.370.

[6] M. Jafari Tadi *et al.*, "A new algorithm for segmentation of cardiac quiescent phases and cardiac time intervals using seismocardiography," presented at the Sixth International Conference on Graphic and Image Processing (ICGIP 2014), Y. Wang, X. Jiang, and D. Zhang, Eds., Beijing, China, Mar. 2015, p. 94432K. doi: 10.1117/12.2179346.

[7] T. Biering-Sørensen *et al.*, "Left ventricular ejection time is an independent predictor of incident heart failure in a community-based cohort," *European J of Heart Fail*, vol. 20, no. 7, pp. 1106–1114, Jul. 2018, doi: 10.1002/ejhf.928.

[8] M. Kaisti *et al.*, "Stand-Alone Heartbeat Detection in Multidimensional Mechanocardiograms," *IEEE Sensors J.*, vol. 19, no. 1, pp. 234–242, Jan. 2019, doi: 10.1109/JSEN.2018.2874706.

[9] Y. D'Mello *et al.*, "Real-Time Cardiac Beat Detection and Heart Rate Monitoring from Combined Seismocardiography and Gyrocardiography," *Sensors*, vol. 19, no. 16, p. 3472, Aug. 2019, doi: 10.3390/s19163472.

[10] T. Hurnanen *et al.*, "Heartbeat Detection Using Multidimensional Cardiac Motion Signals and Dynamic Balancing," in *EMBEC & NBC 2017*, vol. 65, H. Eskola, O. Väisänen, J. Viik, and J. Hyttinen, Eds., in IFMBE Proceedings, vol. 65. , Singapore: Springer Singapore, 2018, pp. 896–899. doi: 10.1007/978-981-10-5122-7_224.

[11] T. Choudhary, L. N. Sharma, and M. K. Bhuyan, "Standalone Heartbeat Extraction in SCG Signal Using Variational Mode Decomposition," in *2018 International Conference on Wireless Communications, Signal Processing and Networking (WiSPNET)*, Chennai: IEEE, Mar. 2018, pp. 1–4. doi: 10.1109/WiSPNET.2018.8538723.

[12] J. Centracchio, S. Parlato, D. Esposito, P. Bifulco, and E. Andreozzi, "ECG-Free Heartbeat Detection in Seismocardiography Signals via Template Matching," *Sensors*, vol. 23, no. 10, p. 4684, May 2023, doi: 10.3390/s23104684.

[13] Y. Chen, W. Xu, W. Zhu, G. Ma, X. Chen, and L. Wang, "Beat-to-beat Heart Rate Detection Based on Seismocardiogram Using BiLSTM Network," in *2021 IEEE 20th International Conference on Trust, Security and Privacy in Computing and Communications (TrustCom)*, Shenyang, China: IEEE, Oct. 2021, pp. 1503–1507. doi: 10.1109/TrustCom53373.2021.00216.

[14] M. Kaisti, M. J. Tadi, O. Lahdenoja, T. Hurnanen, M. Pänkäälä, and T. Koivisto, "Mechanocardiograms with ECG reference." IEEE DataPort, Oct. 05, 2018. doi: 10.21227/VFCS-K196.

[15] M. A. García-González, A. Argelagós-Palau, M. Fernández-Chimeno, and J. Ramos-Castro, "A comparison of heartbeat detectors for the seismocardiogram," in *Computing in Cardiology 2013*, Sep. 2013, pp. 461–464.

[16] K. Munck, "Data for: Multichannel Seismocardiography: An Imaging Modality for Investigating Heart Vibrations." Mendeley, May 19, 2020. doi: 10.17632/SCN464X7XD.1.

[17] C. Yang *et al.*, "An Open-Access Database for the Evaluation of Cardio-Mechanical Signals From Patients With Valvular Heart Diseases," *Front. Physiol.*, vol. 12, p. 750221, Sep. 2021, doi: 10.3389/fphys.2021.750221.

[18] M. Chan, L. Klein, J. Fan, and O. Inan, "SCG-RHC: Wearable Seismocardiogram Signal and Right Heart Catheter Database." PhysioNet. doi: 10.13026/133D-PK11.

[19] M. Nazari and S. M. Sakhaei, "Successive variational mode decomposition," *Signal Processing*, vol. 174, p. 107610, Sep. 2020, doi: 10.1016/j.sigpro.2020.107610.

[20] I. Elnaggar *et al.*, "Multichannel Bed Based Ballistocardiography Heart Rate Estimation Using Continuous Wavelet Transforms and Autocorrelation," in *2022 Computing in Cardiology (CinC)*, 2022, pp. 1–4. doi: 10.22489/CinC.2022.364.

[21] F. Scholkmann, J. Boss, and M. Wolf, "An Efficient Algorithm for Automatic Peak Detection in Noisy Periodic and Quasi-Periodic Signals," *Algorithms*, vol. 5, no. 4, pp. 588–603, Nov. 2012, doi: 10.3390/a5040588.

[22] D. Makowski *et al.*, "NeuroKit2: A Python toolbox for neurophysiological signal processing," *Behavior Research Methods*, vol. 53, no. 4, pp. 1689–1696, Aug. 2021, doi: 10.3758/s13428-020-01516-y.

[23] G. H. Golub and C. F. Van Loan, *Matrix Computations - 4th Edition*. Philadelphia, PA: Johns Hopkins University Press, 2013. doi: 10.1137/1.9781421407944.

[24] S. Parlato, J. Centracchio, D. Esposito, P. Bifulco, and E. Andreozzi, "Heartbeat Detection in Gyrocardiography Signals without Concurrent ECG Tracings," *Sensors*, vol. 23, no. 13, p. 6200, Jul. 2023, doi: 10.3390/s23136200.

[25] T. Choudhary, L. N. Sharma, and M. K. Bhuyan, "Automatic Detection of Aortic Valve Opening Using Seismocardiography in Healthy Individuals," *IEEE J. Biomed. Health Inform.*, vol. 23, no. 3, pp. 1032–1040, May 2019, doi: 10.1109/JBHI.2018.2829608.

[26] T. Choudhary, M. K. Bhuyan, and L. N. Sharma, "A Novel Method for Aortic Valve Opening Phase Detection Using SCG Signal," *IEEE Sensors J.*, vol. 20, no. 2, pp. 899–908, Jan. 2020, doi: 10.1109/JSEN.2019.2944235.